*Arabian Journal of Chemical and Environmental Research*

*Vol. 09 Issue 2 (2022) 168–182*

# Design of Shell and Tube Heat Exchanger for The Production $Co_3O_4$ Nanopowder using Hydrothermal Method

**Ghea Dinda Nugraha[1] Asep Bayu Dani Nandiyanto[2]* Risti Ragadhita[3] and Teguh Kurniawan[4]**

[1]*Departemen of Chemistry, Faculty of Mathematics and Natural Science Education (FPMIPA), Universitas Pendidikan Indonesia, Bandung, Indonesia.*

[2]*Departemen of Chemistry, Faculty of Mathematics and Natural Science Education (FPMIPA), Universitas Pendidikan Indonesia, Bandung, Indonesia.*

[3]*Departemen of Chemistry, Faculty of Mathematics and Natural Science Education (FPMIPA), Universitas Pendidikan Indonesia, Bandung, Indonesia.*

[4]*Department of Chemical Engineering, Faculty of Engineering (FT), Universitas Ageng Tirtayasa, Serang, Indonesia*

*Received 18 November 2022, Revised 20 December 2022, Accepted 25 December 2022*

***Cited as** : G. D. Nugraha, A. B. D. Nandiyanto, R. Ragadhita and T. Kurniawan, Design of Shell and Tube Heat Exchanger for The Production $Co_3O_4$ Nanopowder using Hydrothermal Method, Arab. J. Chem. Environ. Res. 09 (2022) 168-182*

**Abstract**

The purpose of this research is to analyze and develop the application of Heat Exchanger (HE) in the production process of cobalt (II, III) oxide ($Co_3O_4$) nanopowder using hydrothermal method. The type of HE used is the Shell and Tube Heat Exchanger (STHE) type which is designed simply, but still refers to the existing design rules. The specifications of the HE equipment used are shell length of 1.364 m, shell diameter of 0.228 m, inner shell diameter of 0.203 m, inner tube diameter of 0.02119 m, outer tube diameter of 0.0254 m, wall thickness of 0.002108 m, tube length 5.4864 m, tube pitch is 0.03175 m and the number of tubes used is 592 pieces. The results of calculations using Microsoft Excel show that the appropriate design of the heat exchanger on the shell and tube is turbulent flow type, and shows an effectiveness value of 90.35%. The magnitude of the effectiveness value indicates that the STHE design is suitable for the production of $Co_3O_4$ nanopowder. This design is expected as a reference material in designing a heat exchanger to be more economical, effective, and has high reliability.

*Keywords:* $Co_3O_4$ nanopowder, production, hydrothermal method, heat exchanger, effectiveness

*Corresponding author.
*E-mail address:* nandiyanto@upi.edu

ISSN : 2458-6544 

## 1. Introduction

Heat exchanger (HE) is a device used to transfer heat effectively between two gases or liquids from one fluid to another [1,2]. Fluids with different temperatures are separated on the cold side or hot side with a separating medium to achieve optimal thermal conditions in the heat transfer process. HE has been used in various industries including power plants, oil refineries, gas industry, plywood industry, paper industry, food industry and others which mainly use boilers in the production process. Various types of HE are used because of a special requirement. Double tube, shell and tube, fins, plate and shell, cushion plate are some examples of types of heat exchangers used on an industrial scale [3].

Shell and tube heat exchanger (STHE) is one of the most common types of HE that is widely used in various industries [3,4]. According to Master et al., 2003 [5] and Master et al., 2006 [6], more than 30-35% of heat exchangers are STHE types because of their strong geometric construction, easy maintenance, manufacture can be in various sizes, production costs much lower, easy to clean, and considered more flexible when compared to other heat exchangers [7]. Shell and tube type heat exchanger consists of a collection of tubes in a shell, where the fluid flows in the pipes (inside the tube) while the other fluid flows on the outside of the pipe (outside the tube) but still inside the shell. In STHE, liquids with different temperatures pass through a heat exchanger without mixing [8]. Heat transfer occurs between the two fluids, where heat will flow from the higher temperature fluid to the lower temperature fluid.

In industry, cobalt (II, III) oxide ($Co_3O_4$) nanoparticles are used in various applications because of their benefits and excellent properties. Many researchers reported that $Co_3O_4$ has antiferromagnetic properties with an energy band gap of 1.4–1.8 eV and is a p-type semiconductor [9]. $Co_3O_4$ is an interesting material, due to its semiconductor [10], magnetic [11], optical [12], electrochemical [13], and electro-catalytic properties [14]. This material holds promise for applications in electrochromics [15], solar cell energy [16], chemical sensors [17], photocatalytic hydrogen production [18], heterogeneous catalysts [19] and energy storage systems [20]. $Co_3O_4$ nanoparticles are widely applied in gas sensors, data storage, catalysis, electronic components, especially as a lithium-ion battery manufacturing material in the production of mobile phones, computers, notebooks and other electronic products which has resulted in an increase in the demand for these lithium-ion batteries. This causes an increase in the demand for $Co_3O_4$ raw materials.

$Co_3O_4$ nanoparticles can be synthesized and produce various morphologies using different methods. Different synthesis methods will produce different particle sizes, shapes, and structures of $Co_3O_4$ nanomaterials. To date, $Co_3O_4$ nanoparticles with various morphologies such as nanospheres [21, 22], nanowalls [23], nanoflowers [24], nanorods [25-28], nanotubes [29,30], and nanofibers [31] have been

successfully synthesized. Various methods including chemical vapor deposition [32], microwave-assisted process [33], sol-gel [34], wet chemical approach [35], and hydrothermal method [36–38] have been carried out. The hydrothermal method has been widely used because it has various advantages, namely it requires low temperatures, does not need calcination, is inexpensive, has a fairly uniform particle size and morphology, and is especially easy to scale up on an industrial scale [39].

According to previous studies on designing industrial equipment [40, 41] as well as analyzing and evaluating experiments and processes, HE can be used as a production tool in industries such as the organic material industry [40], production of $Fe_3O_4$ nanoparticles [42], production of nano zeolite [43], production of cellulose nanofibrils [44], production of silica [45], and production of carbon [46]. This study aims to design HE for the production of $Co_3O_4$ nanoparticles. HE with shell and tube type is designed. So that it can be useful as a reference in designing HE and become a teaching and learning method for the design process, working mechanism, to HE performance.

## 2. Materials and methods

### 2.1. Synthesis of $Co_3O_4$ Nanopowder

The schematic diagram of the process and PFD in the synthesis of $Co_3O_4$ nanopowder using the hydrothermal method is shown in **Fig 1** and **Fig 2.**

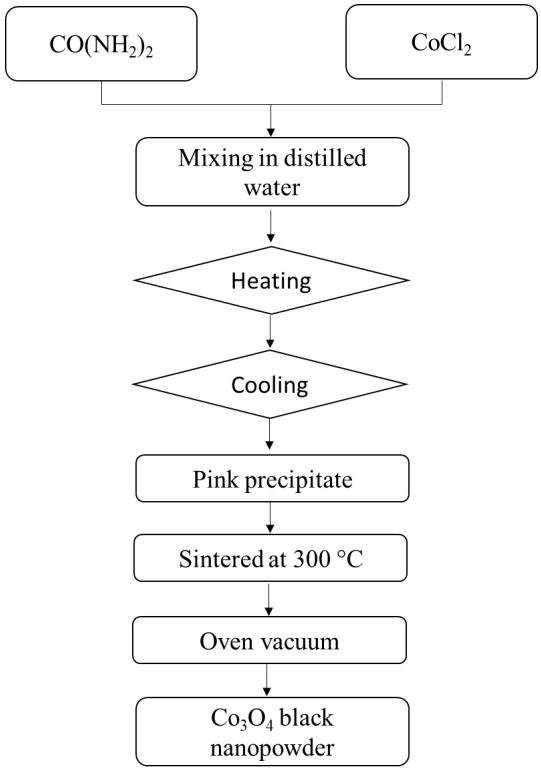


**Figure 1.** Schematic diagram of the synthesis process of $Co_3O_4$ nanopowder

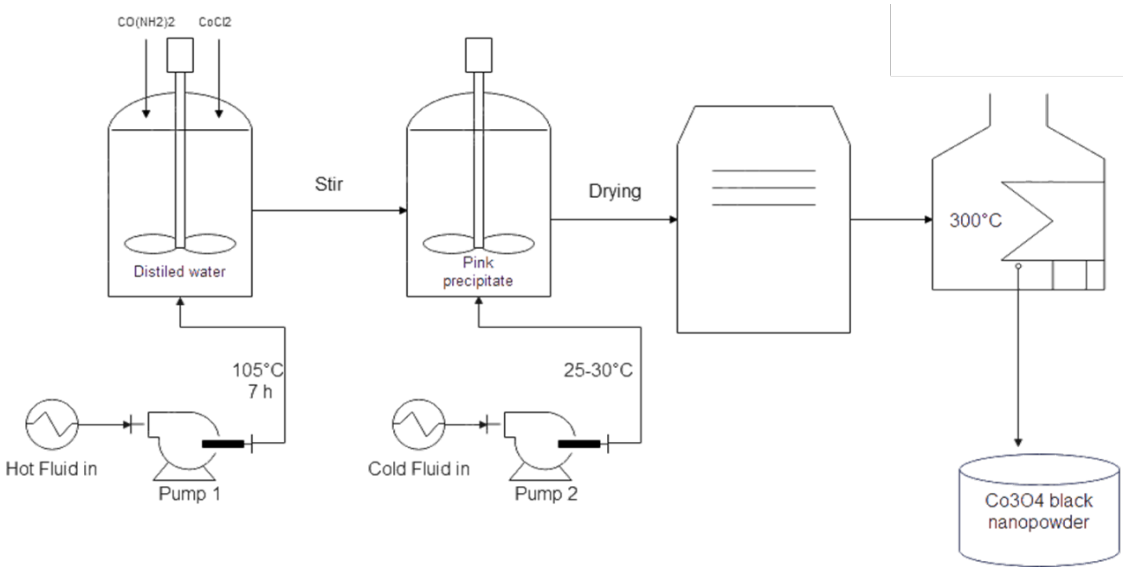


**Figure 2.** PFD on the synthesis process of $Co_3O_4$ nanopowder

The process of making $Co_3O_4$ nanopowder was carried out according to that carried out by Wang et al. (2009). All chemicals used use analytical grade reagents. 1.2 g of cobalt chloride ($CoCl_2$) and 0.06 g of urea ($CO(NH_2)_2$) were dissolved in 20 mL of distilled water until homogeneous. The urea solution is then added dropwise into the $CoCl_2$ solution while continuously stirring. The mixture was then heated to 105°C for 6 hours. After that it was cooled to room temperature, a pink precipitate was produced which was then separated by centrifugation, washed three times with distilled water and ethanol, and dried in a vacuum oven. The dry product was then reheated at 300°C for 3 hours. A black powder is produced, this powder is $Co_3O_4$ successfully synthesized [47].

### 2.2. Mathematical Model for Designing HE

**Table 1** shows the HE parameters to be calculated. The process of collecting data regarding specifications refers to the Standard Tubular Exchanger Manufacturers Association (TEMA), while thermal analysis is in the form of manual calculations using a manual basis using basic Microsoft Office applications based on equations 1-27.

**Table 1.** Calculation of heat exchanger parameters

| No | Section | Parameter | Equation | Eq |
|---|---|---|---|---|
| 1 | Basic Parameters | The energy transferred (Q) | $Q_{in} = Q_{out}$<br>$m_c \times Cp_c \times \Delta T_c = m_h \times Cp_h \times \Delta T_h$<br><br>$Q$ = the energy transferred (Wt)<br>$m$ = the mass flow rate of the fluid (Kg/s)<br>$Cp$ = the specific heat<br>$\Delta T$ = the fluid temperature difference (°C) | (1) |

| | | | | |
|---|---|---|---|---|
| | | Logarithmic mean temperature differenced (LMTD) | $LMTD = \frac{(T_{hi} - T_{Ci}) - (T_{ho} - T_{Co})}{ln\frac{(T_{hi}-T_{Ci})}{(T_{ho}-T_{Co})}}$<br>$T_{hi}$ = the temperature of the hot fluid inlet<br>$T_{ho}$ = the temperature of the hot fluid outlet<br>$T_{Ci}$ = the temperature of the cold fluid inlet<br>$T_{Co}$ = the temperature of the cold fluid outlet<br>All temperature units are in °C | (2) |
| | | Correction factor | $R = \frac{(T_{hi} - T_{ho})}{(T_{Co} - T_{Ci})}$<br>$P = \frac{(T_{Co} - T_{Ci})}{(T_{hi} - T_{Ci})}$<br>$F = \frac{\sqrt{R^2+1}\ln[\frac{1-P}{1-PR}]}{(R-1)\ln(\frac{2-P(R+1-\sqrt{R^2+1}}{2-P(R+1+\sqrt{R^2+1}})}$ | (3)<br>(4)<br>(5) |
| | | Heat Transfer Field Area (A) | $A = \frac{Q}{U \times LMTD}$<br>$Q$ = the energy transferred (W)<br>$U$ = the overall heat transfer coefficient<br>$LMTD$ = the logarithmic mean temperature difference | (6) |
| | | Number of Tubes (N) | $N = \frac{A}{\pi \times D_o \times l}$<br>$N$ = j the number of tubes<br>$A$ = the area of the heat transfer area ($m^2$)<br>$\pi$ = the value of 3.14<br>$D_o$ = the tube diameter (m)<br>$l$ = the tube diameter (m) | (7) |
| | | Shell Diameter | $D_s = 0.63\ (\frac{\sqrt{\frac{CL}{CTP} \times ((A \times (PR)^2 \times D_o}}{l})^{\frac{1}{2}}$<br>$D_s$ = the shell diameter (m)<br>$A$ = the area of the heat transfer area ($m^2$)<br>P,R = the correction factor<br>$D_o$ = the tube diameter (m)<br>$CTP$ = the constant (one tube pass = 0.93; two tube pass = 0.90; and three tube pass = 0.85)<br>$CL$ = the constant (CL at 45 and 90° = 1.00; CL at 30° and 60° = 0.87). | (8) |

| | | | | |
|---|---|---|---|---|
| 2. | Tube | Surface Area of Total Heat Transfer in Tube ($a_t$) | $a_t = N_t \frac{a'_t}{n}$<br>$a_t$ = the total heat transfer surface area in the tube ($m^2$)<br>$N_t$ = the number of tubes<br>$a'_t$ = the flow area in the tube ($m^2$)<br>$n$ = the number of passes. | (9) |
| | | Mass Flow Rate of Water in Tube ($Gt$) | $Gt = \frac{m_h}{a_t}$<br>$Gt$ = the mass flow of water in the tube ($Kg/m^2s$)<br>$m_h$ = = the mass flow rate of the hot fluid (Kg/s)<br>$a_t$ = the flow area tube ($m^2$) | (10) |
| | | Reynold number ($Re_t$) | $Re_t = \frac{di_t \times Gt}{\mu}$<br>$Re_t$ = the Reynolds number in tube<br>$di_t$ = the inner tube diameter (m)<br>$Gt$ = the mass flow of water in the tube ($m^2$)<br>$\mu$ = the dynamic viscosity (Kg/ms) | (11) |
| | | Prandtl Number ($Pr, t$) | $Pr = (\frac{C_p \times \mu}{K})^{\frac{1}{2}}$<br>$Pr$ = Prandtl number<br>$C_p$ = the specific heat of the fluid in the tube<br>$\mu$ = the dynamic viscosity of the fluid in the tube (Kg/ms)<br>$K$ = the thermal conductivity of the tube material (W/m°C) | (12) |
| | | Nusselt number (Nu, t) | $Nu = 0.023 \times {Re_t}^{0.6} \times Pr^{0.33}$ | (13) |
| | | Inside coefficient ($h_i$) | $h_i = \frac{Nu \times K}{d_i, t}$<br>$h_i$ = the convection heat transfer coefficient in the tube (W/m°C)<br>$K$ = the thermal conductivity of the material (W/m°C)<br>$d_i, t$ = the inner tube diameter (m) | (14) |
| 3. | Shell | Shell flow area ($A_s$) | $A_s = \frac{d_s \times C \times B}{P_t}$<br>$D_b = d_o(\frac{N_t}{k_1})^{\frac{1}{n_1}}$<br>$d_s$ = the shell diameter (m)<br>$C$ = clearance ($P_t - d_o$)<br>$B$ = the a shell bundle<br>$P_t$ = the tube pitch ($1.25 \times d_o$) (m) | (15)<br>(16) |

| | | | | |
|---|---|---|---|---|
| | | Mass Flow Rate of Water in Shell ($G_s$) | $G_s = \frac{m_c}{a_s}$<br>$m_c$ = the mass flow rate of the cold fluid (Kg/s)<br>$A_s$ = the shell flow area (m$^2$) | (17) |
| | | Equivalent diameter ($d_e$) | $d_e = \frac{4 \times (\frac{P_t}{2} \times 0.87\ P_t - \frac{1}{2}\pi \frac{d_{o,t}}{4})}{\frac{1}{2}\pi d_{o,t}}$<br>$P_t$ = the tube pitch ($1.25 \times d_o$) (m)<br>$\pi$ = the value of 3.14<br>$d_{o,t}$ = the tube outside diameter (m) | (18) |
| | | Reynold number (Re, s) | $Re_s = \frac{di_t \times Gt}{\mu}$<br>$Re_s$ = the Reynold number<br>$di_t$ = the inner tube diameter (m)<br>$Gt$ = the mass flow of water in the shell (kg/m$^2$s)<br>μ = the dynamic viscosity (Kg/ms) | (19) |
| | | Prandtl Number (Pr, s) | $Pr = \left(\frac{C_p \times \mu}{K}\right)^{\frac{1}{2}}$<br>Pr = the Prandtl number<br>$C_p$ = the specific heat capacity kJ/kg°C<br>μ = the dynamic fluid viscosity (Kg/ms)<br>$K$ = the thermal conductivity (W/m°C) | (19) |
| | | Nusselt number (Nu, s) | $Nu_s = 0.023 \times Re_s^{0.6} \times Pr^{0.33}$<br>$Nu_s$ = the Nusselt number<br>$Re_s$ = the Reynold number<br>Pr = the Prandtl number | (20) |
| | | Convection Heat Transfer Coefficient ($ho$) | $ho = \frac{Nu \times K}{d_e}$<br>$ho$ = the convection heat transfer coefficient (W/m$^2$.°C)<br>$K$ = the thermal conductivity (W/m°C)<br>$d_e$ = the equivalent diameter (m) | (21) |
| 5. | Shell and Tube | Actual Overall Heat Transfer Coefficient ($U_{act}$) | $U_{act} = \frac{1}{\frac{1}{h_i} + \frac{\Delta r}{K} + \frac{1}{h_o}}$<br>$h_i$ = the inside heat transfer coefficient (W/m$^2$.°C)<br>$ho$ = the outside heat transfer coefficient (W/m$^2$.°C)<br>Δr = the wall thickness (m)<br>$K$ = the thermal conductivity (W/m°C) | (22) |

| | | | | |
|---|---|---|---|---|
| 6. | Heat rate | Hot Fluid Rate ($C_h$) | $C_h = m_h . Cp_h$<br>$C_h$ = the hot fluid rate (W/°C)<br>$m_h$ = the specific heat capacity (J/kg.°C)<br>$Cp_h$ = the mass flow rate of hot fluid (kg/s) | (23) |
| | | Cold Fluid Rate ($C_c$) | $C_c = m_c . Cp_c$<br>$C_c$ = the cold fluid rate (W/°C)<br>$m_c$ = the specific heat capacity (J/kg.°C)<br>$Cp_c$ = the mass flow rate of cold fluid (kg/s)<br><br>$Q_{maks} = C_{min}(T_{h,i} - T_{c,i})$<br>$Q_{maks}$ = the maximum heat transfer (W)<br>$C_{min}$ = the minimum heat capacity rate (W/°C)<br>$T_{h,i}$ = the temperature of the hot fluid inlet (°C)<br>$T_{c,i}$ = the temperature of the cold fluid inlet (°C) | (24) |
| 7. | Effectiveness | HE Effectiveness ($\varepsilon$) | $\varepsilon = \frac{Q\ act}{Q\ max} \times 100\%$<br>$Q\ act$ = the actual energy transferred (W)<br>$Q\ max$ = the maximum heat transfer (W) | (25) |
| | | Number of Transfer Unit (NTU) | $NTU = \frac{U \times A}{C_{min}}$<br>$U$ = the overall heat transfer coefficien (W/m$^2$.°C)<br>$A$ = the heat transfer area (m$^2$)<br>$C_{min}$ = the minimum heat capacity rate (W/°C) | (26) |
| | | Fouling factor (Rf) | $Rf = \frac{U_a - U_{act}}{U_a \times U_{act}}$<br>$Rf$ = the fouling factor<br>$U_a$ = the overall heat transfer coefficient (W/m$^2$.°C)<br>$U_{act}$ = the actual overall heat transfer coefficient (W/m$^2$ .°C) | (27) |

## 3. Results and discussion

**Table 2** shows the assumptions regarding the characteristics of the hot and cold fluids used in HE. In HE, the principle of equalizing the difference between the incoming hot fluid temperature (Th in) and the incoming cold fluid temperature (Tc in) is used, compared to the effect of the outlet temperature seen. Several assumptions are used for the shell and tube type HE design. Dipropylene glycol/DPG ($C_6H_{14}O_3$) is used as the hot fluid while water ($H_2O$) is used as the cold fluid. The hot fluid enters at 110°C and leaves at 300°C. While the cold fluid enters at a temperature of 130°C and exits at a temperature of 85°C. The incoming DPG flow rate is 33.43 (kg/s) while the incoming water flow rate is

7.0 (kg/s). **Table 3** shows the results of HE design calculations with the specifications of HE equipment used shell length of 1.364 m, shell diameter of 0.228 m, inner shell diameter of 0.203 m, inner tube diameter of 0.02119 m, outer tube diameter of 0.0254 m, wall thickness of 0.002108 m, tube length 5.4864 m, tube pitch 0.03175 m and the number of tubes used is 592 units.

**Table 2.** Data on fluid properties acting on HE

| **Side** | **Shell side** | **Tube side** |
|---|---|---|
| Fluida type | Hot Dipropylene glycol ($T_h$) | Cold Water ($T_c$) |
| Inlet Temperature, Tin (°C) | 110 | 130 |
| Outlet Temperature, Tout (°C) | 300 | 85 |
| Fluid Flow Rate (kg/s) | 33.43 | 7.0 |
| Operating Pressure (atm) | 1 | 1 |
| Heat Capacity, Cp (J/kg°C) | 4184 | 2180 |
| Density, ρ (kg/m$^3$) | 1022 | 1000 |

The result of the calculation shows that the transferred energy value (Q) in the shell and tube type HE design is 1317015 W. The Reynolds number (Re) in this HE design shows a value of 2610.09. The Re number refers to the ratio between the effects of inertia and viscosity in the flow. So that a flow in the pipe depends on the value of Re. The type of flow that occurs in the shell and tube here is turbulent flow because the value of Re > 2300 [48]. Turbulent flow is a fluid flow in which the particles move randomly and unstable resulting in the flow lines between the fluid particles intersecting each other [49]. So that the characteristics of turbulent flow are obtained, namely irregular fluid paths, mixed flow, high fluid velocity, large flow scale length and low viscosity. Turbulent flow has many uses in industrial processes, in other words most industrial HE uses turbulent flow, which has a higher heat convection coefficient than laminar flow and results in better heat transfer rates [48].

Types of shell and tube HE here are single tube pass, type E, triangular tube layout with single segmental baffle type. Based on the calculation results, the percentage of HE effectiveness is 90.36%. The HE effectiveness shows the actual heat transfer rate divided by the maximum possible heat transfer rate [50]. The magnitude of the effectiveness value indicates that this design is suitable for the production of Co3O4 nanoparticles. The results of the STHE design are in line with previous studies [44-46]. The resulting effectiveness value, measuring the amount of heat carried will be high if the temperature difference between the input and output temperatures is large. So, it can also be interpreted that the effective value of HE is directly proportional to the magnitude of the temperature difference (ΔTLMTD) [51]. The value of TLMTD obtained is 100.669 °C.

**Table 3.** HE specifications based on calculation results

| No | Parameter | Result |
|---|---|---|
| 1 | Type of heat exchanger | Single tube pass, type E shell and tube heat exchanger |
| 2 | Tube outside diameter, (OD) | 0.025 m |
| 3 | Tube inner diameter, (ID) | 0.021 mm |
| 4 | Pitch | 0.031 mm |
| 5 | Total tube number, (Nt) | 510 |
| 6 | CTP | 0.93 |
| 7 | CL | 0.87 |
| 8 | Area of Heat Transfer (A) | 155.05 $m^2$ |
| 9 | Total Heat Transfer Surface Area in Tube ($a_t$) | 0.44 $m^2$ |
| 10 | Mass Flow Rate of Water Fluid in Tube ($Gt$) | 112.09 kg/ $m^2$.s |
| 11 | Reynold Number Tube ($Re_t$) | 2610.09 |
| 12 | Prandtl Number Tube (Pr, t) | 6.27 |
| 13 | Nusselt Number Tube (Nu, t) | 30.45 |
| 14 | Convection Heat Transfer Coefficient in the Tube ($h_i$) | 5517.52 W/ $m^2$. °C |
| 15 | Tube layout | Rotated triangular |
| 16 | Bundle Shell (Db) | 0.527 m |
| 17 | Equivalent Diameter ($d_e$) | 25.83 m |
| 18 | Total Heat Transfer Surface Area in shell ($a_s$) | 0.020 $m^2$ |
| 19 | Mass Flow Rate of Water Fluid in Shell ($G_s$) | 1607.70 kg/ $m^2$.s |
| 20 | Reynold Number Shell (Re, s) | 553804.45 |
| 21 | Prandtl Number Shell (Pr, s) | 977.87 |
| 22 | Nusselt Number Shell (Nu, s) | 16678.67 |
| 23 | Convection Heat Transfer Coefficient in Shell ($ho$) | 709761.26 W/ $m^2$. °C |
| 24 | Overall Heat Transfer Coefficient Actual ($U_{act}$) | 7,8344 W/ $m^2$. °C |
| 25 | Baffle type | Single-segmental |
| 26 | Baffle spacing, B (mm) | 220.4 |
| 27 | Initial Heat Transfer Rate (Q) | 1317015 |
| 28 | Logarithmic Mean Temperature Difference (LTMD) | 100.70°C |
| 29 | Area of Heat Transfer ($m^2$) | 155.05 |
| 30 | HE Effectiveness (**ε**) | 90.35 |
| 31 | Number of Transfer Unit (NTU) | 1.53 |

The performance of this HE is determined by the density, viscosity, thermal conductivity and specific heat of the fluid used. Another factor that affects HE performance is the number and spacing of baffles

in the HE specification. A close baffle distance will increase the effectiveness of HE and a small percentage of baffle cut will increase the effectiveness of HE [52-54].

## Conclusion

Based on the calculations that have been carried out, it can be concluded that the results of the shell and tube type HE design with specifications are shell length of 1.364 m, shell diameter of 0.228 m, inner shell diameter of 0.203 m, inner tube diameter of 0.02119 m, outer tube diameter of 0.0254 m , wall thickness of 0.002108 m, tube length 5.4864 m, tube pitch 0.03175 m and the number of tubes used is 592 pieces indicating an effectiveness value of 90% which is large enough so that it is suitable for the production of Co3O4 nanopowder. Therefore, the shell and tube type HE that has been designed can meet the requirements and standards that have been set.

## Conflict of Interest

This study was conducted without any commercial or financial relationship with any institution.

## References

[1] R. K. Shah and D. P. Sekulic; Fundamentals of heat exchanger design; John Wiley & Sons, 2006.

[2] K. Manjunath and S. C. Kaushik, “Second law thermodynamic study of heat exchangers: A Review,” Renewable and Sustainable Energy Reviews, vol. 40, pp. 348–374, 2014.

[3] U. Salahuddin, M. Bilal, and H. Ejaz, “A review of the advancements made in helical baffles used in shell and tube heat exchangers,” International Communications in Heat and Mass Transfer, vol. 67, pp. 104–108, 2015.

[4] Z. Duan, F. Shen, X. Cao, and J. Zhang, “Comprehensive effects of baffle configuration on the performance of heat exchanger with helical baffles,” Nuclear Engineering and Design, vol. 300, pp. 349–357, 2016.

[5] B. I. Master, K. S. Chunangad, and V. Pushpanathan, “Fouling and fouling mitigation on heat exchanger surfaces,” Fundamentals and Applications, Santa Fe, 2003.

[6] B.I. Master, K.S. Chunangad, A.J. Boxma, D. Kral, P. Stehlík, Most frequently used heat exchangers from pioneering research to worldwide applications,” *Heat Transfer Engineering,* 27 no.6: 4–11 (2006).

[7] M. Mirzaei, H. Hajabdollahi, and H. Fadakar, “Multi-objective optimization of shell-and-tube heat exchanger by constructal theory,” *Applied Thermal Engineering,* vol. 125, pp. 9–19, 2017.

[8] V. V. Prasad Dubey, R. R. Verma, P. S. Verma, A. K. Srivastava, “Performance Analysis of Shell & Tube type heat exchanger under the effect of varied operating conditions,” *IOSR Journal*

*of Mechanical and Civil Engineering*, 11, no. 3: 08–17 (2014).

[9] B. Maddah, J. Shamsi, M. J. Barsang, and M. Rahimi-Nasrabadi, "The chemiluminescence determination of 2-chloroethyl ethyl sulfide using luminol–agno3–silver nanoparticles system," Spectrochimica Acta Part A: Molecular and Biomolecular Spectroscopy, 142: 220–225 (2015).

[10] M. Y. Nassar and I. S. Ahmed, "Hydrothermal synthesis of cobalt carbonates using different counter ions: An efficient precursor to nano-sized Cobalt Oxide (co3o4)," *Polyhedron,* 30 no.15: 2431–2437 (2011).

[11] L. M. Apátiga and V. M. Castaño, "Magnetic behavior of Cobalt Oxide Films prepared by pulsed liquid injection chemical vapor deposition from a metal-organic precursor," *Thin Solid Films*, 496, no. 2: 576–579 (2006).

[12] S. G. Kandalkar, J. L. Gunjakar, C. D. Lokhande, and O.-S. Joo, Synthesis of cobalt oxide interconnected flacks and nano-worms structures using low temperature chemical bath deposition, *Journal of Alloys and Compounds,* 478, no. 1-2: 594–598 (2009).

[13] C. Zhu, G. Saito, T. Akiyama, Urchin-like hollow-structured cobalt oxides with excellent anode performance for lithium-ion batteries, *Journal of Alloys and Compounds,* 646: 639–646, (2015).

[14] R. Hallaj, K. Akhtari, A. Salimi, and S. Soltanian, "Controlling of morphology and electrocatalytic properties of cobalt oxide nanostructures prepared by potentiodynamic deposition method," Applied Surface Science, vol. 276, pp. 512–520, 2013).

[15] K. K. Purushothaman, B. Sethuraman, M. P. Anupama, M. Dhanasankar, and G. Muralidharan, "Optical, structural, and electrochromic properties of Cobalt Oxide Films prepared via the sol–gel route," Materials Science in Semiconductor Processing, vol. 16, no. 6, pp. 1410–1415, 2013).

[16] M. Chen, L.-L. Shao, Z.-M. Gao, T.-Z. Ren, and Z.-Y. Yuan, "Cobalt oxide and nitride particles supported on mesoporous carbons as composite electrocatalysts for dye-sensitized solar cells," Journal of Power Sources, vol. 286, pp. 82–90, 2015).

[17] R. A. Soomro, K. R. Hallam, Z. H. Ibupoto, A. Tahira, S. T. H. Sherazi, S. S. Memon, and M Willander, "Amino acid assisted growth of CuO nanostructures and their potential application in electrochemical sensing of organophosphate pesticide" *Electrochimica Acta,* 190,: 972-979 (2016)

[18] P. A. Mangrulkar, M. M. Joshi, S. N. Tijare, V. Polshettiwar, N. K. Labhsetwar, and S. S. Rayalu, "Nano cobalt oxides for photocatalytic hydrogen production" International journal of hydrogen energy, vol. 37(13), pp. 10462-10466, 2012).

[19] P. Rybak, B. Tomaszewska, A. Machocki, W. Grzegorczyk, and A. Denis, "Conversion of ethanol over supported cobalt oxide catalysts" Catalysis today, vol. 176(1), pp. 14-20, 2011).

[20] M. Zhang, R. Li, X. Chang, C. Xue, and X Gou, "Hybrid of porous cobalt oxide nanospheres and

nitrogen-doped graphene for applications in lithium-ion batteries and oxygen reduction reaction" Journal of Power Sources, vol. 290, pp. 25-34, 2011).

[21] T. He, D. Chen, X. Jiao, Y. Xu, and Y Gu, "Surfactant-assisted solvothermal synthesis of Co3O4 hollow spheres with oriented-aggregation nanostructures and tunable particle size" Langmuir, vol. 20(19), pp. 8404-8408, 2004).

[22] J. Park, X. Shen, and G. Wang, "Solvothermal synthesis and gas-sensing performance of Co3o4 Hollow Nanospheres," *Sensors and Actuators B: Chemical*, vol. 136, no. 2, pp. 494–498, 2009).

[23] T. Yu, Y. W. Zhu, X. J. Xu, Z. X. Shen, P. Chen, C.T. Lim, C.H Sow, Controlled growth and field-emission properties of cobalt oxide nanowalls, *Advanced Materials,* 17(13): 1595-1599 (2005)

[24] Z. Zhu, X. Li, Y. Zeng, W. Sun, W. Zhu, and X. Huang, "Application of cobalt oxide nanoflower for direct electrochemistry and electrocatalysis of hemoglobin with ionic liquid as enhancer", *The Journal of Physical Chemistry C,* vol. 115(25), pp. 12547-12553, 2011).

[25] S. Lian, E. Wang, L. Gao, and L Xu, "Fabrication of single-crystalline Co3O4 nanorods via a low-temperature solvothermal process" Materials Letters, vol. 61(18), pp. 3893-3896, 2007).

[26] S. Sun, X. Zhao, M. Yang, L. Ma, and X Shen, "Facile and eco-friendly synthesis of finger-like Co3O4 nanorods for electrochemical energy storage" *Nanomaterials*, *5*(4): 2335-2347 (2015).

[27] H. Zhang, J. Wu, C. Zhai, X. Ma, N. Du, J. Tu, and D. Yang, "From cobalt nitrate carbonate hydroxide hydrate nanowires to porous Co3O4 nanorods for high performance lithium-ion battery electrodes" *Nanotechnology*, 19(3): 035711 (2007).

[28] M. M. Durano, A. H. Tamboli, and H. Kim, "Cobalt oxide synthesized using urea precipitation method as catalyst for the hydrolysis of sodium borohydride" *Colloids and Surfaces A: Physicochemical and Engineering Aspects*, 520: 355-360 (2017).

[29] X. W. Lou, D. Deng, J. Y. Lee, J. Feng, and L. A. Archer, "Self‐supported formation of needlelike Co3O4 nanotubes and their application as lithium‐ion battery electrodes" *Advanced Materials*, 20(2) : 258-262 (2008).

[30] J. Xu, L. Gao, J. Cao, W. Wang, Z. Chen, "Preparation and electrochemical capacitance of cobalt oxide ($Co_3O_4$) nanotubes as supercapacitor material" *Electrochimica Acta,* 56(2): 732-736, (2010).

[31] Z. Mao, M. Zhou, K. Wang, W. Wang, H. Tao, K. Jiang, "Electrospinning synthesis of $Co_3O_4$ nanofibers as a high-performance anode for sodium ion batteries". *RSC advances,* 7(37): 23122-23126 (2017).

[32] E. P. Koumoulos, V. Markakis, V. P. Tsikourkitoudi, C. A. Charitidis, N. Papadopoulos, and E. Hristoforou, "Tribological characterization of chemical vapor deposited Co and Co3O4 thin films

for sensing reliability in engineering applications" *Tribology International,* 82 : 89-94 (2015).

[33] S. H. Jhung, T. Jin, Y. K. Hwang, and J. S. Chang, "Microwave effect in the fast synthesis of microporous materials: which stage between nucleation and crystal growth is accelerated by microwave irradiation?" *Chemistry–A European Journal*, 13(16): 4410-4417 (2007)

[34] G. A. Santos, C. M. Santos, S. W. da Silva, E. A. Urquieta-González, and P. P. C. Sartoratto, Sol–gel synthesis of silica–cobalt composites by employing $Co_3O_4$ colloidal dispersions, *Colloids and Surfaces A: Physicochemical and Engineering Aspects*, 395: 217-224 (2012).

[35] Y. Li, B. Tan, and Y. Wu, "Mesoporous $Co_3O_4$ nanowire arrays for lithium ion batteries with high capacity and rate capability" *Nano letters,* 8(1): 265-270 (2008).

[36] F. Liu, H. Su, L. Jin, H. Zhang, X. Chu, and W. Yang, "Facile synthesis of ultrafine cobalt oxide nanoparticles for high-performance supercapacitors" *Journal of colloid and interface science*, 505: 796-804 (2017).

[37] G. Wang, X. Shen, J. Horvat, B. Wang, H. Liu, D. Wexler, and J. Yao, "Hydrothermal synthesis and optical, magnetic, and supercapacitance properties of nanoporous cobalt oxide nanorods" *The Journal of Physical Chemistry C,* 113(11): 4357-4361 (2009).

[38] S. K. Meher, and G. R. Rao, "Ultralayered Co3O4 for high-performance supercapacitor applications" *The Journal of Physical Chemistry C,* 115(31): 15646-15654 (2011).

[39] M. Shandilya, R. Rai, and J. Singh, "Hydrothermal technology for smart materials" *Advances in Applied Ceramics,* 115(6): 354-376 (2016).

[40] A. B. D. Nandiyanto, R. Andika, M. Aziz, and L. S. Riza, "Working volume and milling time on the product size/morphology, product yield, and electricity consumption in the ball-milling process of organic material" *Indonesian Journal of Science and Technology,* 3(2): 82-94 (2018.

[41] A. Sukmafitri, R. Ragadhita, and A. B. D. Nandiyanto, "Disk rotation speed and diameter of impactor in disk mill on particle size distribution from rice husk" *Journal of Engineering Science and Technology*, 15(3):1698-1704 (2020).

[42] A.S. Nugraha, A.B.D. Nandiyanto, Design of Shell and Tube Heat Exchanger for Magnetite ($Fe_3o_4$) Particle Production Process, *Indonesian Journal of Multidiciplinary Research,* 3(1): 1-10 (2021)

[43] N.T.D. Hidayah, A.B.D. Nandiyanto, "Shell and tube heat exchanger design for nano zeolite production process" *International Journal of Research and Applied Technology (INJURATECH),* 1(2): 82-93 (2021).

[44] H.N. Purnamasari, T. Kurniawan, and A.B.D. Nandiyanto, "Design of shell and tube type heat exchanger for nanofibril cellulose production process" *International Journal of Research and*

*Applied Technology (INJURATECH),* 1(2): 94-105, (2021).

[45] A. B. D. Nandiyanto, S. R. Putri, R. Ragadhita, R. Maryanti, and T. Kurniawan, "Design of heat exchanger for the production of synthesis silica" Journal of Engineering Research, (2021).

[46] A. B. D. Nandiyanto, S. R. Putri, R. Ragadhita, and T. Kurniawan, "Design of Heat Exchanger for The Production of Carbon Particles" *Journal of Engineering Science and Technology,* 17(4): 2788-2798 (2022).

[47] B. Wang, S. Wang, Y. Tang, Y. Ji, W. Liu, and X. Y. Lu, "Hydrothermal synthesis of mesoporous Co3O4 nanorods as high capacity anode materials for lithium ion batteries" *Energy Procedia,* vol. 158: 5293-5298 (2019).

[48] A. Barun, and E. Rukmana, "Analisis Performansi Pada Heat Exchanger Jenis Sheel and Tube Tipe Bem Dengan Menggunakan Perubahan Laju Aliran Massa Fluida Panas (Mh)" SINTEK JURNAL: *Jurnal Ilmiah Teknik Mesin,* 1(1): (2007).

[49] A. Hasanpour, M.Farhadi, and K. Sedighi, "A review study on twisted tape inserts on turbulent flow heat exchangers: The overall enhancement ratio criteria" *International communications in heat and mass transfer,* 55: 53-62 (2014).

[50] J. Y. San, C. H. Hsu, and S. H. Chen, "Heat transfer characteristics of a helical heat exchanger" *Applied Thermal Engineering*, 39: 114-120, 2012).

[51] B. Sreedhar Rao, C. Keerthana Reddy, P. Meena, and S. Kishore Kumar, "Thermal performance of corrugated plate heat exchanger using ethylene glycol as test fluid" *Journal of Mechanical and Energy Engineering*, 4: (2020).

[52] M. H. Mohammadi, H. R. Abbasi, A. Yavarinasab, H. Pourrahmani, Thermal optimization of shell and tube heat exchanger using porous baffles, *Applied Thermal Engineering,* 170: 115005 (2020)

[53] M.A. Alazwari, M.R. Safaei, Combination Effect of Baffle Arrangement and Hybrid Nanofluid on Thermal Performance of a Shell and Tube Heat Exchanger Using 3-D Homogeneous Mixture Model. *Mathematics*, 9 : 881 (2021). https://doi.org/10.3390/math9080881

[54] Y. Wang, Y. Li, J. Chen, Q. Li and W. Cai, Numerical investigation on flow and heat transfer characteristics of supercritical methane–ethane mixture in a straight channel, *Science and Technology for Energy Transition* 77, 12 (2022). https://doi.org/10.2516/stet/2022012